DUBLIN CITY UNIVERSITY

MICROELECTRONICS RESEARCH LABORATORY

Synchrotron X-Ray Topography (SXRT) Studies of Silicon Wafers & MESA Diodes

(CERN 98-1)

Informal Report

Performed for F. Lemeilleur & A. Ruzin

CERN,

Switzerland.

by

Dr. Patrick J. McNally, Microelectronics Research Laboratory, School of Electronic Engineering, Dublin City University, Dublin 9, Ireland.

1. Introduction

This small report outlines details of experiments performed at HASYLAB, Germany for CERN during the period 31 August - 7 September 1998. The aim of these experiments was to use a technique known as Synchrotron X-Ray Topography to ascertain defect/dislocation distributions and/or strain concentrations within a number of silicon wafers and processed MESA p(i)n diodes for potential use as detector materials or devices.

For future records a description of the sample follows below:

Device Name	Remarks	Resistivity	Impurity	Growth Method
P260--1	Std. FZ Si (Ref. Matl.)	2200	Standard	Float Zone
P260-2	Std. FZ Si (Ref Matl.)	2200	Standard	Float Zone
P527-1	Carbon II Matl.	1900	Carbon II	Float Zone
I100-2	Sn enriched Si	130	Tin	Float Zone
I75-2	O jet enriched, low ρ	500	Oxygen	Float Zone
I208-1	O jet enriched, high ρ	1400	Oxygen	Float Zone
I29P-1	EPI Si, t_{epi}=145 μm	4600	Standard	EPI
P44-B-73	Standard MESA	2200	Standard	Float Zone
P44-B-74	Standard MESA	2200	Standard	Float Zone
P400-B-9	Standard MESA on Carbon I Matl.	2200	Carbon I	Float Zone
P402-B-20	Non-std. MESA Process - N_2 + slow temp ramp	2200	Carbon I	Float Zone
P402-B-21	Non-std. MESA Process - N_2 + slow temp ramp	2200	Carbon I	Float Zone
P402-B-22	Non-std. MESA Process - N_2 + slow temp ramp	2200	Carbon I	Float Zone

All samples first used 30/06.98.

The pictures which appear here have been generated on a system comprising of a high-quality Zeiss microscope, 35 mm camera using high resolution Technical Pan film, or alternatively with a CCD camera, frame-grabber and appropriate software. Some of the images have been processed using a software package called Visilog®, in order to improve clarity. The next section consists of a brief description of SXRT and an outline of the results then follows.

2. Synchrotron X-Ray Topography (SXRT)

X-Ray Topography (XRT) is a non-destructive technique, which can provide a map of the strain or defect distribution in crystals. This technique is based on the difference in reflecting power between perfect and distorted parts of a crystal. It is sensitive to strain fields extending over more than several micrometers and therefore XRT is mainly used for the study of strain, dislocations, planar defects, stacking faults, domain walls in ferroelectric and magnetic materials, growth defects or large precipitates.

Localized imperfections may act as independent scattering centres e.g. small angle scattering by small precipitates or thermal diffuse scattering, but it is the *strains* they induce which modify the diffraction of X-rays by the good crystal. This is essential to an understanding of the mechanism of defect imaging. The image of a dislocation line, for instance, on an X-ray topograph (or in electron microscopy) is not an enlargement of the "core" of the dislocation. By core is meant that inner region surrounding the defect where continuous elasticity is no longer valid and which has a diameter of a few Ångstrøms. Rather, the strains due to the dislocation perturb the crystal for several microns from the defect from the X-Ray aspect (~10 nm from the electron beam aspect), and it is these regions far from the core, which give rise to the defect image, through a deviation from the ideal Bragg reflection observed in the more perfect crystalline regions.

Geometrical resolution is governed by the incident beam local divergence on the sample and usually lies in the micron range. In fact, wavelength and angular spread of the incident beam, together with its lateral extension, are crucial parameters in X-ray topography. Synchrotron radiation X-ray beams provide low divergence beams, which, given their very high intensity, provide for excellent X-ray topographs.

Two main experimental set-ups were used as described below:

(a) White Beam Topography in Large Area Topography Mode (LAT)

This is one of the most commonly used techniques, and provides for an improvement over conventional Lang topography in that the traversal stage can be eliminated. When a single crystal is immersed in a white X-ray beam a number of lattice planes (hkl) select out of the continuous spectrum the proper wavelengths to be reflected according to Bragg's Law:

$$2d_{hkl}.\sin\theta_B = n\lambda \qquad (1)$$

where d_{hkl} is the interplanar spacing of (hkl) lattice planes, θ_B is the Bragg angle, and n is an integer. A beam diffracted in a certain direction $2\theta_B$ with respect to the incident beam has a spectrum of wavelengths λ, λ/2, λ/3, etc. corresponding to diffraction lattice planes (hkl), (2h 2k 2l), (3h 3k 3l) etc. The fundamental reflection hkl or its harmonics may, however, be structure factor forbidden. This is the well-known Laue method.

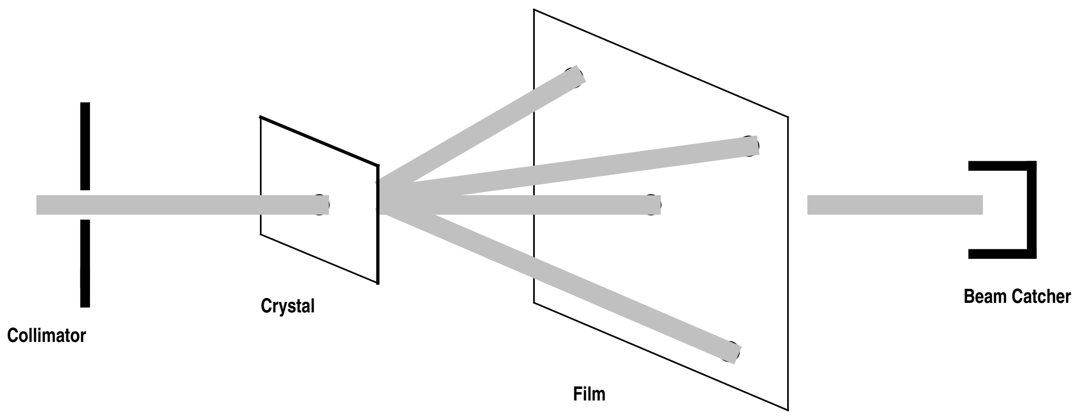

However, due to the low divergence of the synchrotron radiation beam, each spot of this particular Laue pattern is itself a high-resolution topograph. There are a number of significant advantages pertaining to this technique:

(i) There is no need for accurate positioning of the sample; for most studies a fraction of a degree is sufficient compared to a few seconds of arc in the Lang camera. Perfect stability is required only during the exposure, which lasts a few tens of seconds instead of hours.

(ii) There is no need for scanning since the instantaneous image is two-dimensional. However, a compromise has to be found between the image area and the resolution: for a large area the photographic plate should be located far from the sample to avoid spot overlapping, which leads to degradation of the resolution.

(iii) Several spots may be simultaneously recorded corresponding to different reflecting (hkl) planes. In favourable cases, an instantaneous Burgers vector assignment is possible with a judicious choice of the crystal orientation.

(b) White Beam Topography in Section Topography Mode (ST)

An arrangement similar to that for Large Area Topography is used, only in this case the incoming beam is collimated into a narrow ribbon by a slit typically 10-15µm in width. A set of Laue case section topograph images of sample cross-sections are produced as previously described and, provided that the Bragg angle is not too small, the image gives detailed information about the energy flow within the crystal and direct depth information on the defects present in a particular crystal slice. The imaging mechanism for just one reflection is shown below.

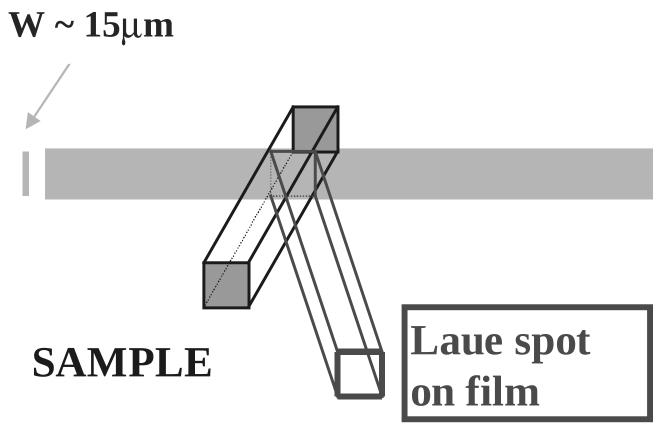

The measurements were performed at HASYLAB-DESY, Hamburg, Germany (Hamburger Synchrotronstrahlungslabor am Deutschen Elektronen-Synchrotron), utilising the continuous spectrum of synchrotron radiation from the DORIS storage ring bending magnet. The ring operated at a positron energy of 4.45GeV and at typical currents of 70-150mA. The aforementioned Laue pattern of topographs was recorded on Kodak SO-343 High-Resolution Professional X-ray film having an emulsion grain size of about 0.05µm. In transmission section topography, the beam was limited by a horizontal slit having a width of 15µm. The beam length was ~8.5 mm and the distance from the sample to the film was ~50 mm. The surface of the wafer made an angle of 72^{o} with the beam. As noted earlier, this method used a transmission geometry, i.e. the diffracted beam passed through the wafer.

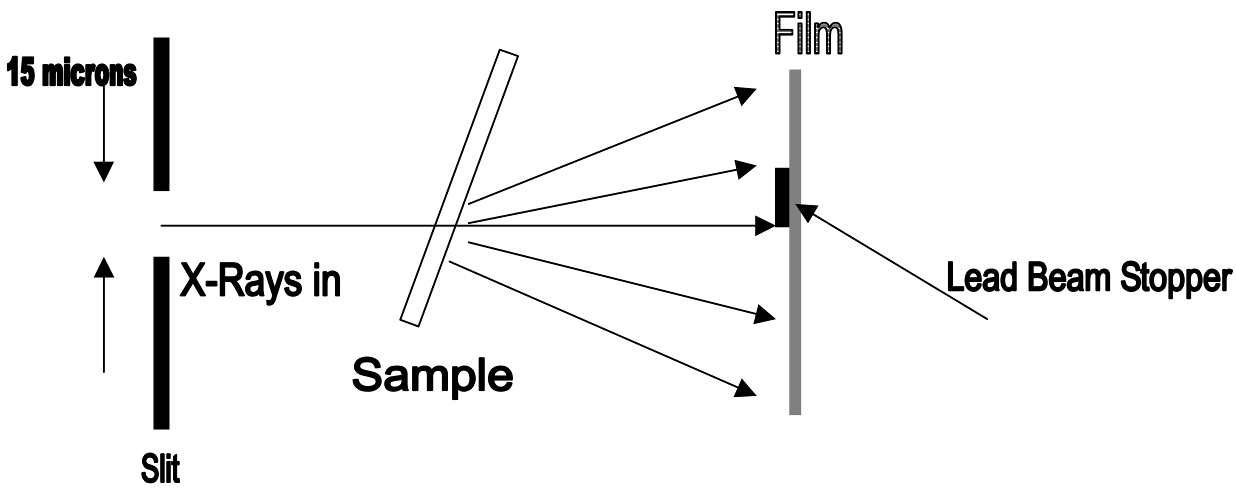

For LAT the beam size was set to 3 mm x 1 mm.

3. **Results**

Figure 1 shows details from a selection of $15\bar{1}$ section topographs for the virgin wafer samples. These images manage to capture details within a slice of each wafer, all the way from the top surface of the wafer (Arrow T in Figure 1a) through to the back side of the wafer (Arrow B in Figure 1a). In all section topographs in this report the top surface (i.e. the surface from which the x-rays exit) is shown uppermost.

The images for all of these wafers appear to be reasonably similar. The main feature in each is the appearance of Pendellösung Fringes, which are the series of black-and-white lines running parallel to the sample surfaces (indicated by dotted lines in Figure 1b). These are not actually related to features within the samples. Rather, they are due to the constructive and destructive interference between the propagating direct and diffracted wave fields within the crystal.

However, it must be pointed out that this phenomenon is only observed for **perfect** or **near-perfect crystals**. It can be safely concluded that for these wafers, there are few precipitates or dislocations present, as these would destroy the Pendellösung Fringes. The presence of these small defects, which may be too small or of too high a density to be imaged individually, can be detected from the destruction of the wave field phase relationships and the resulting absence of Pendellösung Fringes [See e.g. *"High Resolution X-Ray Diffractometry and Topography"*, D.K. Bowen and B.K. Tanner, Taylor & Francis, UK, 1998].

Samples P260-2 and I208-1 also produced similar results.

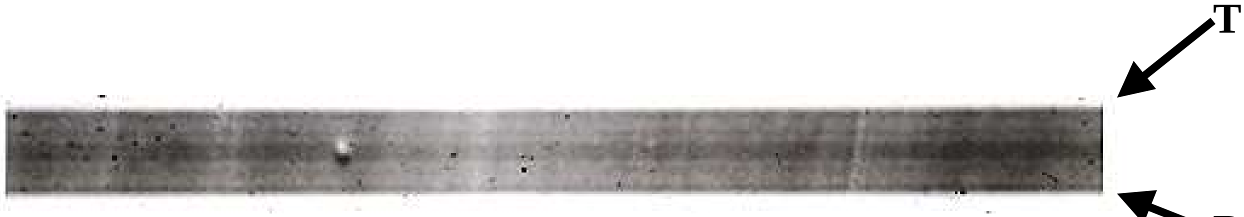

(a) P260-1

(b) P527-1

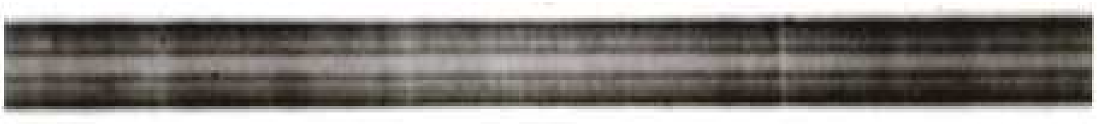

(c) I100-2

(d) I75-2

Figure 1

Section topographs were taken both near the centre of each wafer and near the wafer edge in each case. No differences as a function of location were observed.

However, the situation was dramatically different for the EPI sample I29P-1. Figure 2 is a 220 section topograph taken at a location near the centre of the wafer. Note that we only had a wafer quarter, but nonetheless assumed that the location A, indicated below, corresponded to a region near the wafer centre:

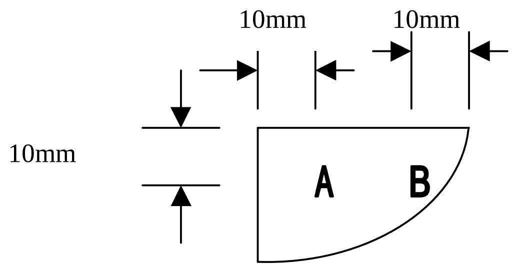

Another topograph was taken near the wafer edge at location B.

In Figure 2 relatively little is seen within the silicon wafer. Pendellösung Fringes are present indicating good quality crystal. The 220 section topograph in Figure 3 is for the same EPI-Si sample, only this time at location B. The change is very dramatic. Large dislocation structures are observed which lie at a depth of ~25-40% of the wafer thickness from the top surface. Upon taking another section topograph just a few millimetres to the right of Location B, we found a region which had both a very good quality region (RHS of Figure 4) wherein sharp Pendellösung Fringes are observed, and an adjacent region containing these dislocation structures (LHS of Figure 4). Note the destruction of the Pendellösung Fringing in this imperfect crystalline region, as previously described.

Returning to Figure 3, it appears that these dislocation features increase in average depth as one proceeds from the left-hand side to the right-hand side of the ~4 mm length of this image.

One question remains: what exactly are these features? Since they appear to lie approximately parallel to the nominal epilayer-substrate interface and are generally at the same nominal depth, one may postulate that these may be **misfit dislocations and accompanying threading dislocations** due to strain relaxation. This was confirmed by an analysis of Figure 5, which is a $2\bar{4}2$ Large Area Topograph of the misfit dislocated region at the wafer edge. The size of the imaged region is ~3 mm x 1 mm, and please remember that this is a transmission projection topograph. Our hypothesis is confirmed by the presence of long dislocation lines, which appear to propagate in three main directions (indicated by lines 1,2 and 3 in Figure 5). The section topographs also appear to confirm that the misfit dislocations are not solely confined to the epilayer-substrate interface, but are accompanied by threading dislocations which permit these to access the upper and lower surfaces of the wafer. This is suggested by the presence of white-line features running upwards and downwards from the "black-dot" images of the dislocation lines themselves. One possible view of this mechanism is shown below. However, confirmation of this will require further studies.

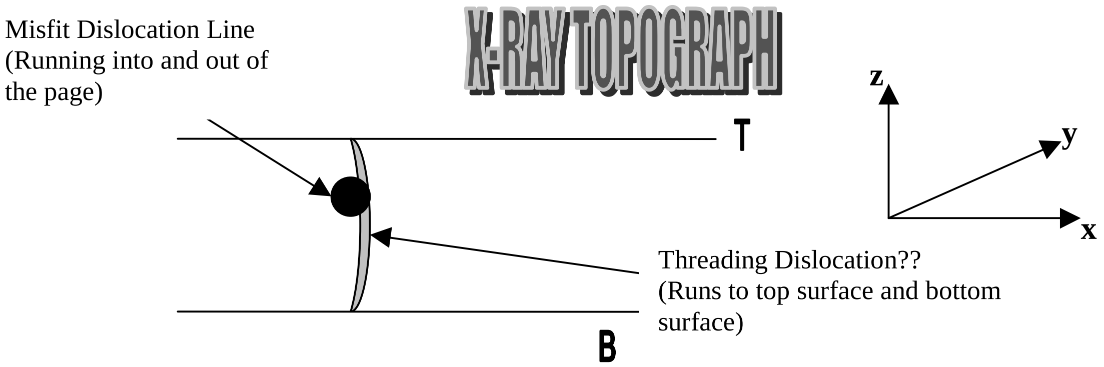

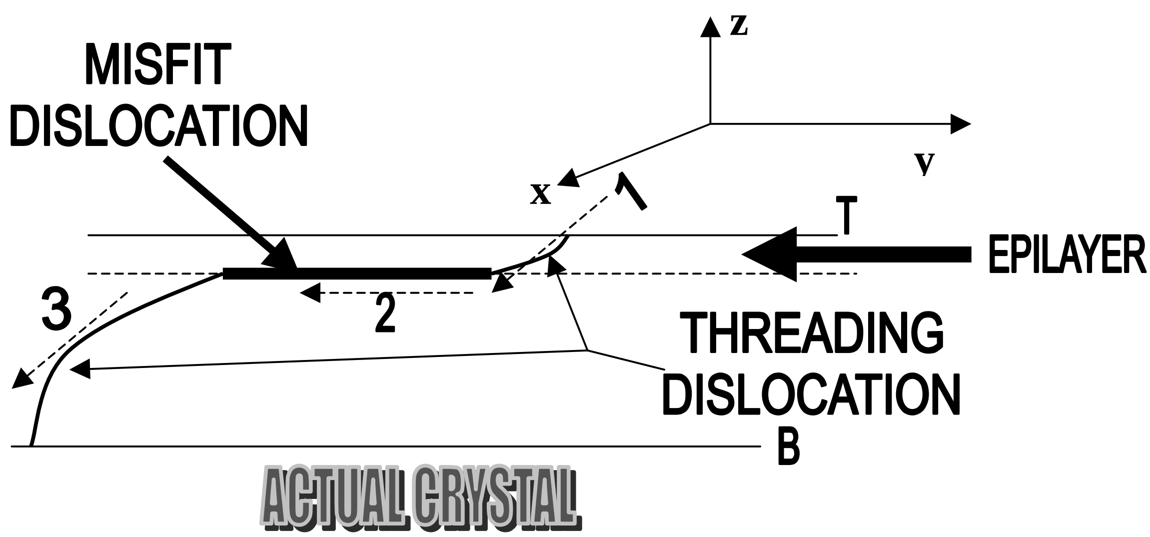

Dislocation propagation directions 1,2 and 3 correspond to those indicated in Figure 5

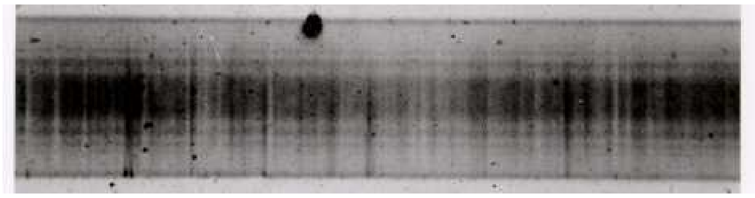

Figure 2 (I29P-1-A)

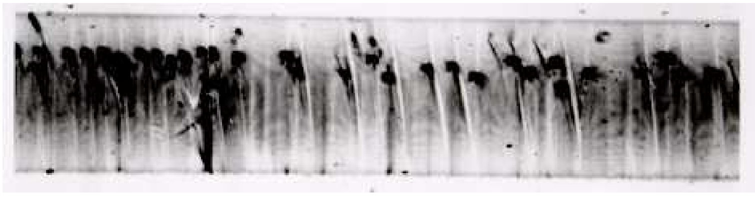

Figure 3 (I29P-1-B (Region 1))

Figure 4 (I29P-1-B (Region 2))

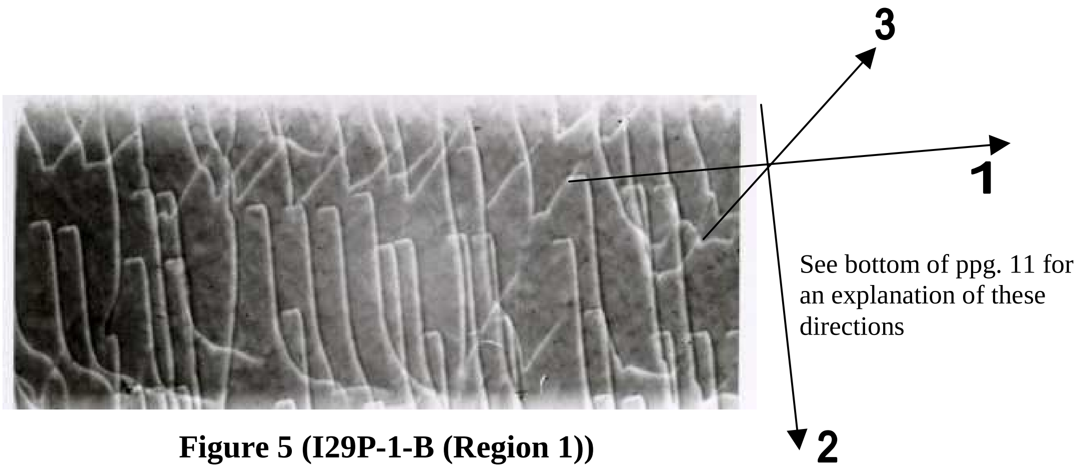

Figure 5 (I29P-1-B (Region 1))

The next sets of images are topographs of the MESA diode samples, both in section and large-area modes. Figures 6a and 6b are 022 section and $2\bar{4}2$ large area projection topographs, respectively, for the samples P44-B-73 and P44-B-74. These are the standard MESA processes diodes. The section topographs reveal significant dislocation/defect generation, though many of these do not appear to be individually resolved. The occurrence of these defects is clustered, as evidenced by the mottled grey-and-white appearance of the silicon within the bulk of the wafer. Dark (lower x-ray intensity recorded on the film) regions most likely correspond to dislocated or defect-rich regions, while the lighter regions most likely correspond to more defect-free regions. This is confirmed by the large area topograph, an example of which is shown in Figure 6c for P44-B-74.

Note also the very high misorientation in the silicon near the upper and lower surfaces. This is seen as an apparent "lifting up" of the images of the diffracting silicon with respect to the remaining diffracting materials, i.e. the streaks indicated by Arrows C in Figures 6a & b. The most plausible cause of this is increased strain near the surfaces due to the metallization process and possible amorphisation due to thermal processing/annealing of these metal contacts.

No discernable differences are observed between these two samples.

Figure 6a (P44-B-73)

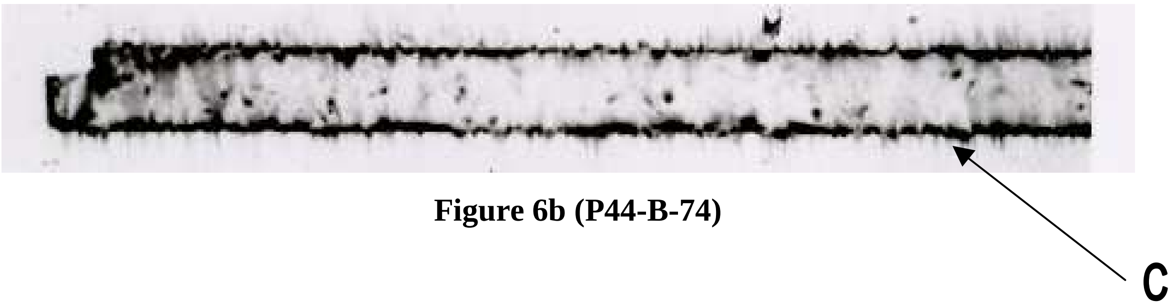

Figure 6b (P44-B-74)

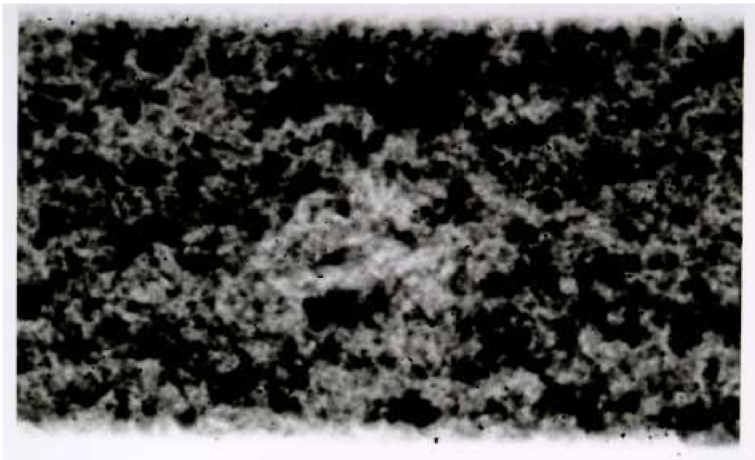

Figure 6c (P44-B-74)

Figures 7a and 7b are similar section and large area topographs for sample P400-B-9. While generally similar to the standard diodes a number of new features are now observed. Firstly, the section topographs reveal many more small black dots throughout the bulk of the silicon, and are indicated by Arrows D in Figure 7a. These may be due to the presence of agglomerates or precipitates, which have now been nucleated or created by the thermal processing.

The large area topograph of Figure 7b also reveals diffuse, though still unmistakable, linear features which run along the direction indicated by the lines on the right-hand side of this figure. Their origin is uncertain.

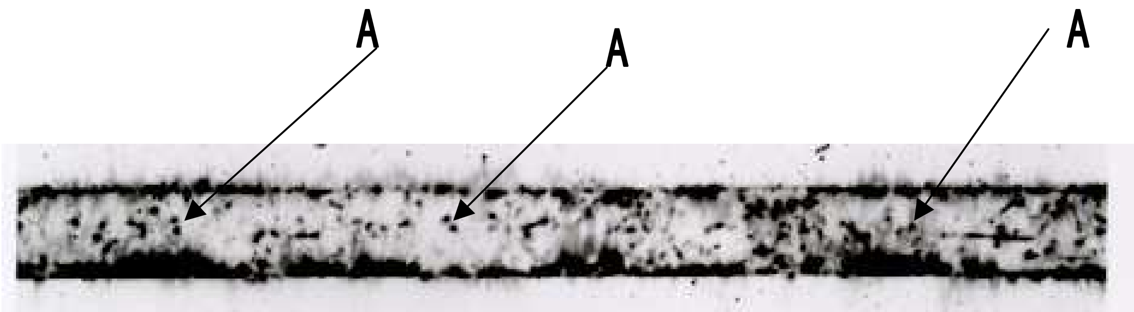

Figure 7a (P400-B-9)

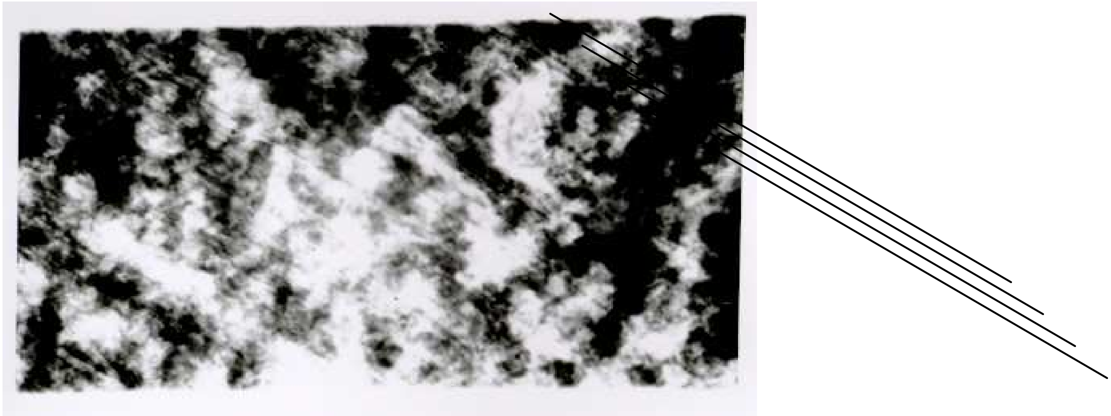

Figure 7b (P400-B-9)

The last diode type to be studied was the non-standard MESA on Carbon I material using a N_2 ambient and a slow temperature ramp, i.e. samples P-402-B-20, P402-B-21 and P402-B-22. Very little difference was seen between these samples, so only a few representative topographs are shown below. Figure 8a is a 022 section topograph for this type of sample (P402-B-21) and Figure 8b is a $2\bar{4}2$ large area topograph.

A smaller number of the precipitates/agglomerations are found in these samples and the overall quality of the silicon is better than for any of the other MESA diodes, including the standard diodes. This is most clearly seen by comparing Figure 8b to all the previous large area topographs. Some diffuse line structures may also be present, though they are very unclear. The lines on the right-hand side of Figure 8b may be a useful aid in visualising these. Once again their significance is unknown at this point in time.

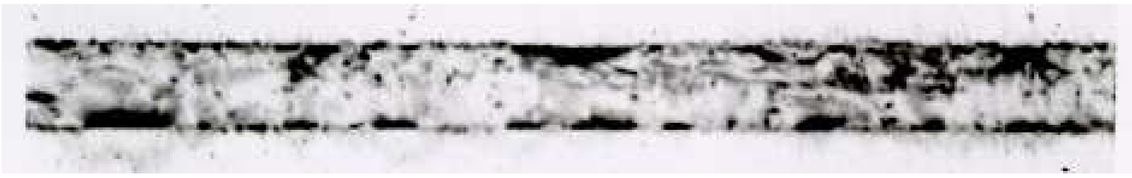

Figure 8a (P402-b-21)

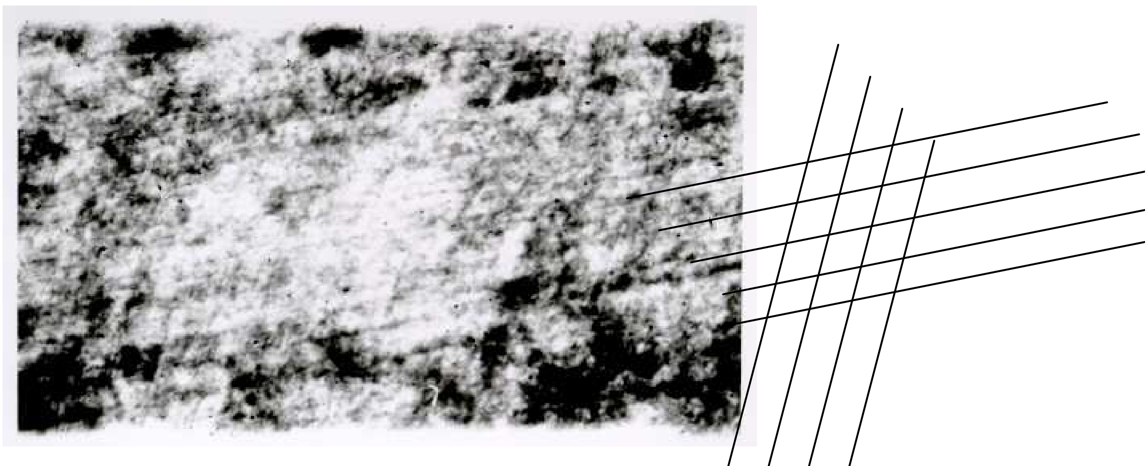

Figure 8b (P402-b-21)